Extraction of radiative and nonradiative rates in Sb based midwave infrared lasers using a novel approach

Ahmed I. Lobad,[1,a)] E. A. Pease,[2,b)] L. R. Dawson,[2] Sanjay Krishna,[2] and L. A. Vern Schlie[3]
[1]*Boeing LTS, Albuquerque, New Mexico 87117, USA*
[2]*Center for High Technology Materials, University of New Mexico, Albuquerque, New Mexico 87106, USA*
[3]*Directed Energy Directorate, Air Force Research Laboratory, Albuquerque, New Mexico 87117, USA*

(Received 17 May 2007; accepted 18 February 2008; published online 18 March 2008)

We developed a technique using nonlinear correlation of photoluminescence (PL) to characterize midwave infrared lasers by extracting the density and temperature dependence of the carrier lifetime and its exact branching into radiative and nonradiative processes. This was accomplished, *without time resolving the PL recovery*, through mathematical optimization. We extracted this information by using a laser source that can be operated in both continuous-wave and short pulse modes. Through fitting of the PL signal and its nonlinear correlation for both laser modes of operation, the carrier lifetime as a function of density is extracted. As a proof of principle, we investigated a midinfrared Sb based laser and showed that the radiative branching ratio drops from ~54% at 80 K to about 3% at room temperature, resulting from an order of magnitude increase in the nonradiative rate coupled with a factor of 2 reduction in the radiative rate. We believe that this is a very generic approach and can be extended to various luminescing material systems. © *2008 American Institute of Physics.* [DOI: 10.1063/1.2894310]

I. INTRODUCTION

Midwave infrared (MWIR) lasers and detectors operating in the range of 2–5 μm are in great need for wide range of applications such as remote sensing, LADAR, detection of chemical warfare agents, intelligence, surveillance and reconnaissance, missile tracking and infrared countermeasures. The most promising technology for fabricating MWIR lasers employs antimonide based materials. Electronic and optoelectronic devices based on GaSb substrates have been a subject of active research in the past few years.[1–4] In the past, Sb based optically pumped lasers have been reported on GaSb substrates using a metamorphic buffer grown with digital alloys.[5] These are "As-free" lasers and are based on a type-I alignment in the InGaSb/InAlSb system. Using a digital alloy buffer layer terminating with $Al_{.73}In_{.27}Sb$ as the "substrate," a multiquantum well active region using AlGaInSb barriers and $Ga_{.6}In_{.4}Sb$ wells demonstrates both photoluminescence and intense cw laser emission at 2.5 μm under optical pumping by a 980 nm pump laser at room temperature.

Accurate characterization of the recombination processes in these structures is indispensable for guiding and optimizing the growth process toward the goal of achieving room temperature MWIR lasers and detectors. The relevant time constants range from nanoseconds to tens of nanoseconds, which makes time resolved techniques based on mechanical delay stages impractical. This is due to the significant variation of the laser beam spot size and misalignment involved along the delay path length. Alternatively, while fast MIR detectors capable of resolving dynamics down to ~30 ns do exist, they do not provide information on the radiative and nonradiative processes involved. In this paper, we report on a novel technique to extract the radiative and nonradiative processes as a function of carrier density in these lasers using nonlinear correlation of photoluminescence. This was accomplished by using *a laser source that can be operated in both a continuous-wave and short pulse modes*. Through fitting of the PL signal and its nonlinear correlation for both laser modes of operation, the carrier lifetime and radiative branching ratio were extracted as a function of density. The pulse repetition rate in the short pulse mode acts as a reference clock in the fitting procedure for achieving effective time resolution. We believe that this is a very generic approach and can be extended to various luminescing material systems.

II. EXPERIMENTAL SETUP AND MEASUREMENTS

The samples for this study were grown by solid source molecular beam epitaxy. The growth is initiated by a 0.5 μm thick AlSb layer. To allow the growth of As-free light-emitting materials, the digital alloy buffer layer, consisting of alternating thin (tens of angstroms) layers of $Al_{1-y}In_ySb$ and $Al_{1-z}In_zSb$ is grown on the AlSb nucleation layer, where y, z, and thickness are chosen to provide the desired average In content. After the growth of a suitable number of periods of such material, typically corresponding to a total thickness of 5000 Å, the thickness ratio is changed to correspond to an increase in the average In content, usually in steps of about 9% or 10%. There are no threading dislocations visible in cross sectional transmission electron microscopy images, indicating that at least the region close to the top of the buffer layer has very few dislocations. The active region

[a)]Electronic mail: ahmed.lobad@kirtland.af.mil.
[b)]Presently at Tau Technology, Albuquerque, New Mexico.

Report Documentation Page

Form Approved
OMB No. 0704-0188

1. REPORT DATE	2. REPORT TYPE	3. DATES COVERED
2008		**00-00-2008 to 00-00-2008**

4. TITLE AND SUBTITLE	5a. CONTRACT NUMBER
Extraction of radiative and nonradiative rates in Sb based midwave infrared lasers using a novel approach	5b. GRANT NUMBER
	5c. PROGRAM ELEMENT NUMBER
6. AUTHOR(S)	5d. PROJECT NUMBER
	5e. TASK NUMBER
	5f. WORK UNIT NUMBER
7. PERFORMING ORGANIZATION NAME(S) AND ADDRESS(ES) **University of New Mexico,Center for High Technology Materials,Albuquerque,NM,87106**	8. PERFORMING ORGANIZATION REPORT NUMBER
9. SPONSORING/MONITORING AGENCY NAME(S) AND ADDRESS(ES)	10. SPONSOR/MONITOR'S ACRONYM(S)
	11. SPONSOR/MONITOR'S REPORT NUMBER(S)

12. DISTRIBUTION/AVAILABILITY STATEMENT
Approved for public release; distribution unlimited

13. SUPPLEMENTARY NOTES

14. ABSTRACT

15. SUBJECT TERMS

16. SECURITY CLASSIFICATION OF:			17. LIMITATION OF ABSTRACT	18. NUMBER OF PAGES	19a. NAME OF RESPONSIBLE PERSON
a. REPORT	b. ABSTRACT	c. THIS PAGE			
unclassified	**unclassified**	**unclassified**	**Same as Report (SAR)**	**6**	

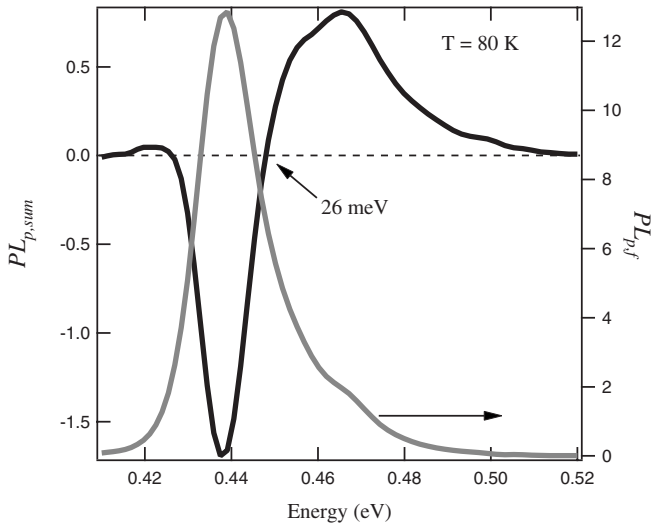

FIG. 1. 80 K photoluminescence traces at fundamental frequency ($PL_{p,f}$) and sum frequency ($PL_{p,sum}$) spectra taken at 70% of the maximum average excitation power ($N_{max} \sim 1.3 \times 10^{11}$ cm^{-2}). The sum frequency correlation spectrum has a zero crossing at excess energy $\varepsilon_0 \sim 26$ meV above the band edge.

consists of three compressively strained ($\sim 0.6\%$) $In_{0.4}Ga_{0.6}Sb/Al_{0.2}In_{0.49}Sb$ wells grown on $Al_{0.55}In_{0.45}Sb$ buffer.

We used a Clark-MXR erbium doped fiber laser generating subpicosecond pulses separated by $T_{pp}=24$ ns at 1.55 μm with ~ 60 mW average power. The laser is additively pulse mode locked using a combination of polarizers and birefringent wave plates. By judicious adjustment of one waveplate, the laser can be reliably switched between mode locked and cw operation of similar average power $\bar{P}$. Under pulsed excitation, using pulses that are orders of magnitude shorter than the carrier recombination time, the initial carrier density n_0 is proportional to the energy per pulse ($n_0 \propto \bar{P} \cdot T_{pp}$). On the other hand, the carrier density under cw excitation is proportional to the average power divided by the density dependent recombination rate $n_{cw} \propto \bar{P}/\rho(n_0)$, where $\rho(n_0)$ is the inverse lifetime.

The laser beam was split into two equal beams that were modulated using one chopper wheel at different frequencies ($\omega_1=400$ Hz, $\omega_2=333$ Hz). Both beams travel an equal path length to the sample insuring temporal coincidence for pulsed operation. The two beams were combined on the sample with a 10 cm focal length lens producing a maximum incident power density of ~ 400 W/cm^2. The luminescence was then collected and focused on an InSb cooled detector. The signal was fed into two lock-in amplifiers to simultaneously measure the correlation signal $PL_{i,sum}$ at the sum frequency ω_{sum} and $PL_{i,f}$ at a fundamental frequency ω_f (ω_1 or ω_2), where the index $i=p$ or cw for pulsed or cw excitation, respectively. A long-pass filter (>2.4 μm) was used to block the stray laser excitation wavelength. Using a Janis cryostat, luminescence measurements were taken at room temperature and 80 K. The average laser excitation power was changed over two orders of magnitude. Figure 1 shows the 80 K time-integrated luminescence spectra for $PL_{p,sum}$ and $PL_{p,f}$ taken at 70% of the maximum excitation power ($n=0.7N_{max}$). Due to the nonlinearity of the occupation Fermi function, the correlation spectrum changes sign from negative (saturation) to positive (superlinear). This zero crossing occurs at an energy ε_0 that is proportional to the Fermi energy.

We used the zero-crossing energy (ε_0) in the correlation spectrum ($PL_{p,sum}$) of Fig. 1 to extract the excited carrier density. Following Chilla *et al.*, the time-integrated spectrum at low temperature for short pulse excitation of an initial carrier density n and for an effective density of states g is given by $PL(n,\varepsilon) \propto \ln(n/g\varepsilon)$.[6] By solving for the zero-crossing energy of the correlation spectrum which can be approximated as $PL_{sum}(n,\varepsilon)=PL(n,\varepsilon)-2PL(n/2,\varepsilon)$, we obtain $\varepsilon_0 \sim 0.25(n/g)$. From Fig. 1, $\varepsilon_0=26$ meV (above the band edge) and using an effective density of states of $g \sim 10^{12}$ cm^{-2} eV^{-1},[7] we obtain $n \sim 10^{11}$ cm^{-2} and a maximum carrier density used in this work $N_{max} \sim 1.5 \times 10^{11}$ cm^{-2}.

The measured $PL_{i,j}$ ($i=p$, cw; $j=f$, sum) versus carrier density n_0 (normalized to N_{max}) are plotted in Figs. 2(a) and 2(b) for room temperature and 80 K, respectively. In this case, the cw-excited traces are in effect plotted against a scaled carrier density flux (n_0/T_{pp}). The solid lines represent the curve fits used to extract the recombination rates as will be shown. A common feature of the data (open circles) in both (a) and (b) of Fig. 2 is that $PL_{p,f} > PL_{cw,f}$ for low excitation with $PL_{p,f}$ saturating at higher excitation becoming smaller than $PL_{cw,f}$. For the sum frequency traces (solid circles), $PL_{p,sum}$ turns negative at medium excitation levels, while $PL_{cw,sum}$ stays positive up to high excitation levels. These features result from the difference between the carrier density levels under pulsed and cw excitations and the functional dependence of radiative and nonradiative recombination rates on these carrier density levels, as will be shown in the discussion below.

III. MODEL SETUP

Luminescence correlation is a powerful technique[6,8–15] that has so far been underutilized due to difficulties in interpreting measurements involving time and energy integrated correlations of temporally and spectrally varying carrier density.[6] This problem of correlations can be avoided by time resolving the nonlinearity of the PL upconversion signal in a nonlinear crystal, in a similar fashion to time resolving the nonlinearity of pump-probe measurements.[16,17] However, it is desirable to avoid dealing with measurements involving several meters of mechanical delay for resolving nanosecond dynamics. Even in the presence of adequate fast detectors that would alleviate the problem of mechanical delay stages, the radiative and nonradiative rates cannot be resolved. Therefore it would be appealing to devise a simple technique to extract these material properties using time and energy integrated PL signal.

A. Quantifying the nonlinear response

Given the sensitivity of the measured photoluminescence (PL) correlations to the nonlinear density dependences, the correct theoretical expressions for luminescence have to be

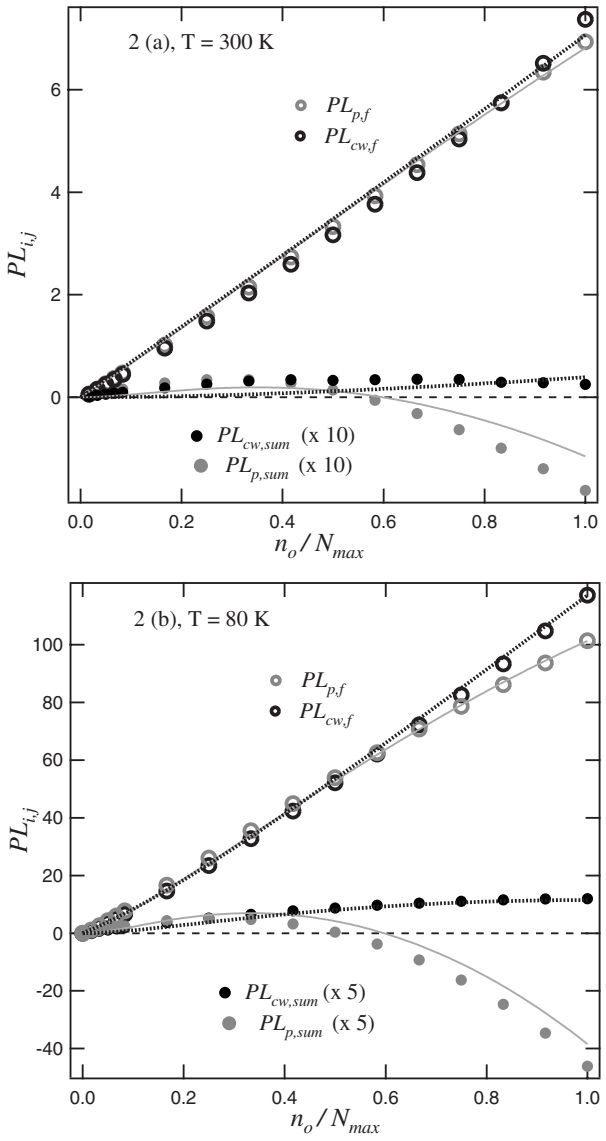

FIG. 2. The measured time-integrated/energy-integrated $PL_{i,j}$ ($i=p,\mathrm{cw}$; $j=f,\mathrm{sum}$) vs the normalized carrier density $n_0/N_{\max}$ ($N_{\max}\sim 1.3\times 10^{11}$ cm^{-2}) for 300 K (a) and 80 K (b). The lower curves (solid circles) are the sum frequency traces scaled by factors of 10 and 5 for 300 and 80 K, respectively. The solid lines are the fitting results. The pulsed data and line fits are in gray while those for cw excitation are in black.

used for reliable extraction of the inverse lifetime $\rho(n)$ and its branching into its radiative $\rho_{\mathrm{r}}(n)$ and nonradiative $\rho_{\mathrm{nr}}(n)$ constituents out of the fitting procedure. Even then, matters are further complicated by the confusion about what is actually measured in a lock-in amplifier and what the nonlinear correlation signal relates to. For example, in a modulation based technique a lock-in measures a quantity proportional to the derivative of a function rather than the value of a function as is conventionally assumed. In the presence of two modulated pump beams, the excited carrier density can be expressed as a constant plus a time varying sinusoidal contribution, $n_{\mathrm{dc}}+n_m(t)=n_0/2+n_0/4\{\sin(\omega_1 t)+\sin(\omega_2 t)\}$, where n_0 is the peak carrier density. In order to determine how the measured sum frequency signal relates to the luminescence function, we expand the PL function as a Taylor series around the dc value,

$$\mathrm{PL}[n_{\mathrm{dc}}+n_m(t)]=\sum_i \frac{n_m(t)^i}{i!}\mathrm{PL}(n_{\mathrm{dc}})^i. \tag{1}$$

By expanding the series one finds that in a lock-in measurement the sum frequency term is equal to $\mathrm{PL}_{\mathrm{sum}}(n_{\max}=n_0)=(n_0^2/32)\partial^2\mathrm{PL}(n_0/2)/\partial n^2$, and the signal measured at one of the fundamental frequencies is given by $\mathrm{PL}_f(n_{\max}=n_0)=(n_0/4)\partial\mathrm{PL}(n_0/2)/\partial n$. Therefore the measured luminescence would be proportional to $\mathrm{PL}(n)$ only if it happens to be a linear function which would then imply zero luminescence correlation. Similarly, expressing the correlation term as $\mathrm{PL}_{\mathrm{sum}}=\mathrm{PL}(2n)-2\mathrm{PL}(n)$ is only correct for square and cubic nonlinearities.

B. Luminescence nonlinearity

For short pulse excitation, the time- and spectrally integrated PL is given by

$$\mathrm{PL}_p(n_0)=c\int_0^{T_{\mathrm{pp}}} N(t)\rho_r[N(t)]dt, \tag{2}$$

where $N(t)$ is the instantaneous carrier density of initial density and n_0 and c is a constant proportional to the collection solid angle and detector efficiency. Through change of variables, time can be eliminated from Eq. (2) using the rate equation $dN/dt=-N\rho(x)$ to obtain

$$\mathrm{PL}_p(n_0)=-c\int_{n_0}^{0} \rho_r(N)/\rho(N)dN. \tag{3}$$

Here we assume the carrier lifetime to be short enough compared to T_{pp} such that there is no constant accumulated background carrier density, which is the case in our sample. Otherwise one has to explicitly take into account the buildup of a background signal as a function of the ratio between the carrier lifetime and the pulse repetition time. Fortunately we do not need to integrate Eq. (3) since the measured quantities are expressed in terms of derivatives of this integral. This gives

$$\mathrm{PL}_{p,f}(n_0)=c\frac{n_0}{4}\frac{\rho_r(n_0/2)}{\rho(n_0/2)}, \tag{4}$$

$$\mathrm{PL}_{p,\mathrm{sum}}(n_0)=c\frac{{n_0}^2}{32}\left[\frac{1}{\rho(n_0/2)}\left.\frac{\partial\rho_r}{\partial n}\right|_{n_0/2}-\frac{\rho_r(n_0/2)}{\rho^2(n_0/2)}\left.\frac{\partial\rho}{\partial n}\right|_{n_0/2}\right]. \tag{5}$$

The cw-excited luminescence signal is measured for the same average power used in pulsed excitation. This allows expressing the cw luminescence signal in terms of the same average carrier flux n_0/T_{pp} used for the pulsed measurements.

$$\mathrm{PL}_{\mathrm{cw}}(n_0/T_{\mathrm{pp}})=n_{\mathrm{cw}}(n_0)\rho_r[n_{\mathrm{cw}}(n_0)]T_{\mathrm{pp}}, \tag{6}$$

$$\mathrm{PL}_{\mathrm{cw},f}(n_0/T_{\mathrm{pp}}) = cT_{\mathrm{pp}}\frac{n_0}{4}\left\{\rho_r\left[n_{\mathrm{cw}}\left(\frac{n_0}{2}\right)\right]\left.\frac{\partial n_{\mathrm{cw}}}{\partial n}\right|_{n_0/2} + n_{\mathrm{cw}}\left(\frac{n_0}{2}\right)\left.\frac{\partial \rho_r(n_{\mathrm{cw}})}{\partial n}\right|_{n_0/2}\right\} \tag{7}$$

$$\mathrm{PL}_{\mathrm{cw,sum}}(n_0/T_{\mathrm{pp}}) = cT_{\mathrm{pp}}\frac{{n_0}^2}{32}\left\{\rho_r\left[n_{\mathrm{cw}}\left(\frac{n_0}{2}\right)\right]\left.\frac{\partial^2 n_{\mathrm{cw}}}{\partial n^2}\right|_{n_0/2} + 2\left.\frac{\partial n_{\mathrm{cw}}}{\partial n}\right|_{n_0/2}\left.\frac{\partial \rho_r(n_{\mathrm{cw}})}{\partial n}\right|_{n_0/2} + n_{\mathrm{cw}}\left(\frac{n_0}{2}\right)\left.\frac{\partial^2 \rho_r(n_{\mathrm{cw}})}{\partial n^2}\right|_{n_0/2}\right\}, \tag{8}$$

where $n_{\mathrm{cw}}, \partial n_{\mathrm{cw}}/\partial n$, and $\partial^2 n_{\mathrm{cw}}/\partial n^2$ can be obtained from the relation $n_{\mathrm{cw}}(n_0)\rho[n_{\mathrm{cw}}(n_0)] = n_0/T_{\mathrm{pp}}$. Note that the dependence of Eqs. (7) and (8) on T_{pp} but not in Eqs. (4) and (5) acts as a reference clock and an anchor in the extraction of $\rho(n)$ by fitting the data to Eqs. (4), (5), (7), and (8).

IV. SOLUTION METHODOLOGY

The treatment so far has been general and applicable for all luminescing materials whether molecular or semiconducting and no specific radiative and nonradiative processes have been assumed. Solving the problem begins by choosing an analytic expression for the radiative and nonradiative rates that reflects the significant processes in the material system used whether Auger, electron transfer quenching, carrier diffusion, etc. In this work, for a semiconducting material, the decay rates were represented by

$$\rho_{\mathrm{r}}(n) = \rho_{\mathrm{r}0} + \rho_{\mathrm{r}1}n + \rho_{\mathrm{r}2}n^2, \tag{9}$$

$$\rho_{\mathrm{nr}}(n) = \rho_{\mathrm{nr}0} + \frac{\rho_{\mathrm{nr}1}n + \rho_{\mathrm{nr}2}n^2}{1 + n/Ns_{\mathrm{nr}}}, \tag{10}$$

$$\rho(n) = \rho_r(n) + \rho_{\mathrm{nr}}(n). \tag{11}$$

These forms allow for simulation of linear, quadratic, and saturating dependence on the carrier density as needed for realistic modeling radiative and Auger processes. Approaching degeneracy, saturation starts to set in for both radiative ($\rho_{\mathrm{r}2} < 0$) (Refs. 18 and 19) and Auger (at Ns_{nr}) (Refs. 20–22) rates. These forms also allow for simulating the effect a constant dopant density has on the PL density dependence. Some of these coefficients could be deemed insignificant in a specific temperature and/or data range as a result of the data fitting procedure.

We solve for the eight parameters of Eqs. (9) and (10) and the unknown parameter c of Eq. (2) by simultaneously fitting the four measured pulsed and cw luminescence curves to their corresponding expressions in Eqs. (4), (5), (7), and (8). In principle it is possible to extract all these parameters from only one of the four curves if data could be acquired with zero laser noise and drift over a large enough range and with the proper density of points. By using all four curves in a simultaneous fitting, we compensate for these experimental limitations. In order to perform this simultaneous fitting, we exploit the orthogonality of sinusoidal functions of different frequencies to form an orthogonal superposition of the four measured curves $\Im_{\mathrm{exp}}(n)$ and fit that to the corresponding orthogonal superposition $\Im(n;\rho_{\mathrm{r}},\rho_{\mathrm{nr}})$ of Eqs. (4), (5), (7), and (8) given by

$$\Im(n;\rho_{\mathrm{r}},\rho_{\mathrm{nr}}) = \mathrm{PL}_{p,f} + \mathrm{PL}_{p,\mathrm{sum}}\sin(10n) + \mathrm{PL}_{\mathrm{cw},f}\sin(40n) + \mathrm{PL}_{\mathrm{cw,sum}}\sin(100n). \tag{12}$$

This insures that the four equations, and their corresponding measured curves, contribute to the error function $[\Im(n;\rho_{\mathrm{r}},\rho_{\mathrm{nr}}) - \Im_{\mathrm{exp}}(n)]$ at different modulation frequencies. Thus enabling us to visually ascertain whether the fitting/minimization result is satisfactory for all four equations or whether the fitting parameters need to be perturbed to allow convergence to a different set that minimizes the overall cost function.

Since there are eight fitting parameters (c, Ns_{nr}, $\rho_{\mathrm{r}i}$, $\rho_{\mathrm{nr}i}$, $i=0,1,2$), the chi-square as a function of the parameter space could be a very rugged terrain with no smooth trajectory toward the absolute minimum. Therefore, it is important to guide the fitting program by narrowing the available parameter space using constraints on the forms of physically acceptable solutions to prevent the optimization routine from being trapped in a local minimum representing a suboptimum or even a nonphysical solution. One such constraint is for the total recombination rate to be a monotonically increasing function of n. A more powerful constraint is formed by forcing the optimum solution to satisfy ratio of measured $\mathrm{PL}_{p,f}$ at two different temperatures. From Figs. 2(a) and 2(b) the average ratio $\mathrm{PL}_{p,f\ \mathrm{at}\ 80\ \mathrm{K}}$ to $\mathrm{PL}_{p,f\ \mathrm{at}\ 300\ \mathrm{K}}$ is roughly ~16. Thus Eq. (4) leads to the following condition to be satisfied by the optimum solution at both temperatures,

$$\frac{\overline{\mathrm{PL}_{p,f}|_{80}}}{\mathrm{PL}_{p,f}|_{\mathrm{RT}}} = \left.\left(\frac{\rho_r}{\rho}\right)\right|_{80\ \mathrm{K}} \times \left.\left(\frac{\rho}{\rho_r}\right)\right|_{300\ \mathrm{K}} \sim 16. \tag{13}$$

For experimental confirmation we time resolved the total recombination time by measuring the correlation as a function of the time delay between the two pump pulses. Taking into account the nonmonotonic dependence (displayed in Fig. 2) of the correlation on the carrier density, the extracted carrier recombination times were 5 ± 0.5 ns at 80 K and 0.8 ± 0.3 ns at 300 K. These values are effectively an average lifetime taken at maximum excitation since the lifetime starts shorter and increases with diminishing carrier density. The optimization routine was executed with various starting parameters close to and far from the above measured recombination times. It was found that only one optimal solution that is consistent with the measured values produces the lowest chi-square fit. Starting from another value more than a factor of 2 away from the measured rate often results in the routine being trapped in a local minimum with a chi-square value of at least seven times that of the optimal solution.

V. DISCUSSION

The extracted recombination functions are plotted in Figs. 3(a) and 3(b) at room temperature and 80 K, respectively, along with the experimentally measured rates. The recombination rates are extracted for carrier density ranging from 0 to $n_{\mathrm{dc}} = n_0/2$ since the coefficients of the Taylor ex-

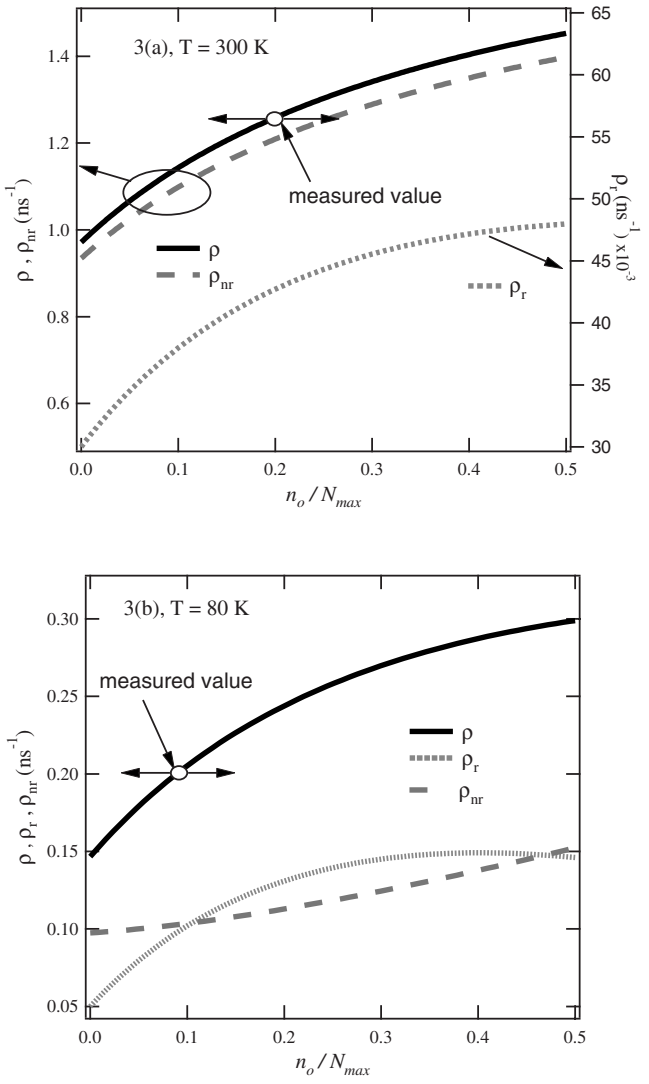

FIG. 3. The extracted recombination functions are plotted for 300 K (a) and 80 K (b) as a function of the normalized carrier density. The measured recombination rates are indicated by the open circles.

pansion in Eq. (1) are expressed in terms of n_{dc}. Several features responsible for the measured cw and pulsed nonlinear responses are evident in the solution. The radiative rate first increases strongly with n_0 and then saturates. Therefore the ratio $\rho_r(n)/\rho(n)$, which is the slope of $PL_{p,f}$, initially increases and then decreases. On the other hand, $PL_{cw,f}$ is determined by the radiative rate at a lower carrier density $n_{cw}(n_0)$ rather than n_0 where $\rho_r(n)/\rho(n)$ increases strongly. That explains the behavior of $PL_{i,f}$ as a function of average power. Similarly, due to the strong saturation of the radiative rate, the PL develops a negative curvature, thus a negative $PL_{p,sum}$, at high carrier density in the pulsed case but not for the cw case where it is determined by the radiative rates in the low density nonsaturating regime. The radiative branching ratio drops from ~54% at 80 K to about 3% at room temperature, resulting from an order of magnitude increase in the nonradiative rate combined with a reduction by a factor of 2 in the radiative rate.

The extracted fitting coefficients along with their standard deviation are listed in Table I for both 300 and 80 K.

TABLE I. The extracted fitting coefficients along with their standard deviation for both 300 and 80 K

300 K	80 K
$\rho_{r0}=0.03\pm0.004$ ns^{-1}	$\rho_{r0}=0.048\pm0.005$ ns^{-1}
$\rho_{r1}=(0.08\pm0.05)/N_{max}$ cm^2 ns^{-1}	$\rho_{r1}=(0.5\pm0.08)/N_{max}$ cm^2 ns^{-1}
$\rho_{r2}=(-0.09\pm0.05)/N_{max}{}^2$ cm^4 ns^{-1}	$\rho_{r2}=(-0.56\pm0.073)/N_{max}{}^2$ cm^4 ns^{-1}
$\rho_{nr0}=0.93\pm0.006$ ns^{-1}	$\rho_{nr0}=0.097\pm0.005$ ns^{-1}
$\rho_{nr1}=(2.1\pm1.0)/N_{max}$ cm^2 ns^{-1}	$\rho_{nr1}=(0.07\pm0.006)/N_{max}$ cm^2 ns^{-1}
ρ_{nr2} is not significant	$\rho_{nr2}=(0.08\pm0.1)/N_{max}{}^2$ cm^4 ns^{-1}
$N_{s_{nr}}=(0.4\pm0.5)N_{max}$ cm^{-2}	$N_{s_{nr}}$ is not significant

Clearly the coefficients are not all equally constrained. The coefficients with the highest confidence are ρ_{r0} and ρ_{nr0} for both 300 and 80 K, whereas those with the least confidence are N_S and ρ_{nr2}. Moreover, the coefficients for the 80 K are, in general, more constrained than those for room temperature. This is reflected in the better curve fits for the 80 K data shown in Fig. 2. In addition, the standard deviation for a particular coefficient is also influenced by the sensitivity of these functions to slight perturbations of that coefficient. Further experimentation with different analytic forms for $\rho_r(n)$ and $\rho_{rn}(n)$ and more efficient optimization techniques will be carried out to maximize the sensitivity to all coefficients involved and to better optimize the solution. Finally, care has to taken during data acquisition to guard against laser drift and beam misalignment since the sum frequency signal is very sensitive to beam spatial overlap.

In conclusion, we report a novel approach to determine the radiative and nonradiative processes in Sb based MWIR lasers using a nonlinear correlation of PL with pulsed and continuous-wave excited PL. Fast decay rates and their temperature variation were extracted using a fitting procedure without resorting to ultrafast detectors or to time resolved techniques involving very long mechanical delay stages. We believe that this is a very generic approach and can be extended to various material systems.

ACKNOWLEDGMENTS

We acknowledge the support of AFOSR and Missile Defense Agency.

[1] L. Esaki, J. Cryst. Growth **52**, 227 (1981).
[2] C. Hilsum and H. D. Rees, Electron. Lett. **6**, 277 (1970).
[3] G. Motosugi and T. Kagawa, Jpn. J. Appl. Phys. **19**, 2303 (1980).
[4] O. Hildebrand, W. Kuebart, and M. H. Pilkuhn, Appl. Phys. Lett. **37**, 801 (1980).
[5] E. A. Pease, L. R. Dawson, A. L. Gray, L. F. Lester, and D. M. Gianardi, J. Appl. Phys. **93**, 3177 (2003).
[6] J. L. A. Chilla, O. Buccafusca, and J. J. Rocca, Phys. Rev. B **48**, 14347 (1993).
[7] I. Vurgaftman, J. R. Meyer, and L. R. Ram-Mohan, J. Appl. Phys. **89**, 5815 (2001).
[8] A. Olsson, D. J. Erskine, Z. Y. Xu, A. Schremer, and C. L. Tang, Appl. Phys. Lett. **41**, 659 (1982).
[9] M. B. Johnson, T. C. McGill, and A. T. Hunter, J. Appl. Phys. **63**, 2077 (1988).
[10] D. W. Liu, X. M. Xu, and Y. F. Chen, Phys. Rev. B **49**, 4640 (1994).
[11] Y. Yamada, T. Mishina, Y. Masumoto, Y. Kawakami, J. Suda, S. Fujita, and S. Fujita, Phys. Rev. B **52**, R2289 (1995).
[12] R. Kumar, A. S. Vengurlekar, and S. S. Prabhu, Solid State Commun. **100**, 287 (1996).

[13] S. Pau, J. Kuhl, M. A. Khan, and C. J. Sun, Phys. Rev. B **58**, 12916 (1998).
[14] I. Reimand and J. Aaviksoo, Phys. Rev. B **61**, 16653 (2000).
[15] B. Pal, A. V. Gopal, S. S. Prabhu, and A. S. Vengurlekar, Phys. Rev. B **65**, 045312 (2002).
[16] A. Lobad and L. A. Vern Schlie, J. Appl. Phys. **95**, 97 (2004).
[17] A. Lobad and L. A. Vern Schlie, J. Appl. Phys. **96**, 4066 (2004).
[18] R. Olshansky, C. B. Su, J. Manning, and W. Powazinik, IEEE J. Quantum Electron. **20**, 838 (1984).
[19] F. Stern, J. Appl. Phys. **41**, 833 (1982).
[20] J. O. Drumm, B. Vogelgesang, G. Hoffmann, C. Schwender, N. Herhammer, and H. Fouckhardt, Semicond. Sci. Technol. **17**, 1115 (2002).
[21] V. Chazapis, H. A. Blom, K. L. Vodopyanov, A. G. Norman, and C. C. Phillips, Phys. Rev. B **52**, 2516 (1995).
[22] A. Haug, Solid-State Electron. **21**, 1281 (1978).